DALTON
FULL PAPER

Synthesis, X-ray structures, electrochemistry, magnetic properties, and theoretical studies of the novel monomeric $[CoI_2(dppfO_2)]$ and polymeric chain $[CoI_2(\mu\text{-}dppfO_2)_n]$

Teresa Avilés,[a] António Dinis,[a] José Orlando Gonçalves,[a] Vitor Félix,[b] Maria José Calhorda,[c,d] Ângela Prazeres,[c] Michael G. B. Drew,[e] Helena Alves,[f] Rui T. Henriques,[g] Vasco da Gama,[f] Piero Zanello[h] and Marco Fontani[h]

[a] *Departamento de Química, Centro de Química Fina e Biotecnologia, Faculdade de Ciências e Tecnologia, Universidade Nova de Lisboa, 2829-516 Caparica, Portugal. E-mail: tap@dq.fct.unl.pt*
[b] *Departamento de Química, Universidade de Aveiro, 3810-193 Aveiro, Portugal. E-mail: vfelix@dq.ua.pt*
[c] *ITQB, UNL, Apartado 127, 2781-901Oeiras, Portugal. E-mail: mjc@itqb.unl.pt.*
[d] *Departamento de Química e Bioquímica, Faculdade de Ciências, Universidade de Lisboa, 1749-016 Lisboa, Portugal*
[e] *Department of Chemistry, University of Reading, Whiteknights, Reading, UK RG6 2AD*
[f] *Departamento de Química, Instituto Tecnológico e Nuclear, Est. Nacional 10, P-2686-953 Sacavém, Portugal*
[g] *Departamento de Engenharia Química, Instituto Superior Técnico, Av. Rovisco Pais, P-1049-001 Lisboa, Portugal*
[h] *Dipartimento di Chimica dell'Università di Siena, Via Aldo Moro, 53100 Siena, Italy*

Received 19th June 2002, Accepted 2nd October 2002
First published as an Advance Article on the web 14th November 2002

The new compound $[Co(\eta^5\text{-}C_5H_5)(dppf\text{-}P,P')I]I$, **1**, was synthesised by the stoichiometric reaction of the Co(III) complex $[Co(\eta^5\text{-}C_5H_5)(CO)I_2]$, **2**, with 1,1′-bis(diphenylphosphino)ferrocene (dppf) in CH_2Cl_2, and was characterised by multinuclear NMR spectroscopy. Exposure to air of THF or CH_2Cl_2 solutions of compound **1** gave, in an unexpected way, a polymeric chain comprising bridging 1,1′-bis(oxodiphenylphosphoranyl)ferrocene ($dppfO_2$) joining tetrahedral Co(II) units $[CoI_2(\mu\text{-}dppfO_2)]_n$, **3**. Attempts to obtain the polymeric chain **3** by the direct reaction of $dppfO_2$ with CoI_2, in CH_2Cl_2, gave instead the monomeric compound $[CoI_2(dppfO_2)]$, **4**, in which $dppfO_2$ is coordinated in a chelating mode. The structural characterisation of compounds **2**, **3**, and **4** was carried out by single crystal X-ray diffraction studies. The magnetic behaviour of $[CoI_2(dppfO_2)]$ and $[CoI_2(\mu\text{-}dppfO_2)]_n$ was studied, and the results are consistent with tetrahedral $S = 3/2$ Co^{II}, possessing a $^4A_2$ ground state, and $S = 0$ Fe^{II}. In these compounds, Co^{II} negative zero field splittings were determined from an analysis of the magnetic susceptibility temperature dependence, with $D/k = -13$ and -14 K for $CoI_2(dppfO_2)$ and $[CoI_2(\mu\text{-}dppfO_2)]_n$, respectively. DFT calculations were performed in order to understand the electronic structure of $[Co(\eta^5\text{-}C_5H_5)(dppf\text{-}P,P')I]I$, **1**, as well as that of the paramagnetic specie $[CoI_2(dppfO_2)]$, **4**. The $[CoI_2(\mu\text{-}dppfO_2)]_n$ chain was also analysed and found to behave very similarly to the monomeric iodine derivative **4**. The calculations showed the unpaired electrons to be localized on the Co(II) centre in all these species. The rather complicated electrochemical behaviour exhibited by the dppf complex $[Co^{III}(\eta^5\text{-}C_5H_5)(dppf\text{-}P,P')I]I$ and by $[Co(dppfO_2)I_2]$ is discussed.

Introduction

Ferrocenylphosphine ligands are currently attracting much attention, mainly because their complexes have applications in homogeneous catalysis and for their potential as redox active ligands. Their usefulness is related to the variety of bonding modes they can exhibit, ranging from chelating one single metal centre, to bridging two or more metals. All these modes are well documented. For instance, 1,1′-bis(diphenylphosphino)-ferrocene (dppf) has been shown to coordinate metal fragments with different geometries and electron counts.[1]

In this work, the coordinating ability of the bulky dppf ligand towards Co(III) precursor complexes was investigated. Some Co(III) complexes containing dppf have already been reported.[2] In the reaction of the Co(III) complex $[Co(\eta^5\text{-}C_5H_5)(CO)I_2]$ with dppf in CH_2Cl_2, the new compound $[Co(\eta^5\text{-}C_5H_5)(dppf\text{-}P,P')I]I$, **1**, was formed. Upon exposure to air, CH_2Cl_2 or THF solutions gave rise unexpectedly to a new polymeric coordination compound of Co(II) of formulation $[CoI_2(\mu\text{-}dppfO_2)]_n$, **3**. There are few transition metal complexes containing $dppfO_2$ as a ligand; only some Cu(I) and Cu(II) complexes have been described.[3] Attempts were made to obtain the polymeric chain $[CoI_2(\mu\text{-}dppfO_2)]_n$ by the direct reaction of CoI_2 and $dppfO_2$, but, instead, the monomeric compound $[CoI_2(dppfO_2)]$, **4**, in which $dppfO_2$ is coordinated to Co(II) in a chelating mode, was formed. Two different coordination modes of the ligand $dppfO_2$, bridging and chelating, are illustrated in this work. The two compounds were structurally characterised by single crystal X-ray diffraction techniques, and their magnetic properties were studied. DFT[4] calculations (ADF program)[5] were performed on several mononuclear species and on a model of the $[CoI_2(\mu\text{-}dppfO_2)]_n$ chain, in order to understand the nature of the frontier orbitals and the properties of these compounds, also in connection with their redox propensity. The

tight-binding approach[6] within the extended Hückel method was used to study the one-dimensional chain.[7]

Results and discussion

Chemical studies

The reaction of equimolar quantities of $[Co(\eta^5\text{-}C_5H_5)(CO)I_2]$, **2**, and dppf in CH_2Cl_2 at room temperature yields brown–red crystals of the new compound $[Co(\eta^5\text{-}C_5H_5)(dppf\text{-}P,P')I]I$, **1**, (see Scheme 1) in *ca.* 80% yield ($\eta^5\text{-}C_5H_5$ = Cp).

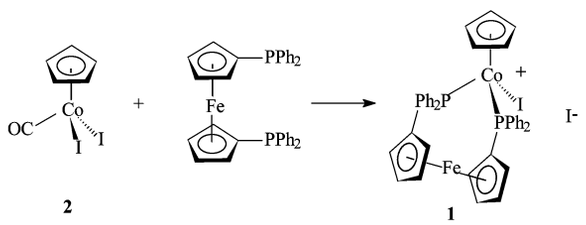

2 **1**

Scheme 1

The ^1H NMR spectrum in $CDCl_3$ shows four singlets at δ 4.27, 4.48, 4.52 and 5.3 for the ferrocenyl ring protons as has been observed in the similar complex $\{[Rh(\eta^5\text{-}C_5H_5)(dppf\text{-}P,P')Cl](PF_6)_2\}$[8] having a chelated structure. The ^{31}P NMR spectrum shows a singlet at δ 47.29. The liquid secondary ion mass spectra ($LSIMS^+$) shows the parent peak at *m*/*z* 805 $[Co(\eta^5\text{-}C_5H_5)(dppf\text{-}P,P')I]^+$ (7%), the base peak $[Co(\eta^5\text{-}C_5H_5)(dppf\text{-}P,P')]^{2+}$ at *m*/*z* 678 (100%) and dppf at *m*/*z* 554 (30%). So far and after several attempts, we have been unable to grow crystals suitable for X-ray structural determination. This reaction is similar to the one described for $Co(\eta^5\text{-}C_5H_5)(CO)I_2$ with bis(tertiary phosphines).[9] Exposure of THF or CH_2Cl_2 solutions of **1** to air results in a colour change from red–brown to green in one or two days; from the green solutions green crystals can be obtained. The reaction was repeated several times and although a colour change was always observed, it was difficult to obtain crystals in all cases, and the yields were erratic. The green crystals obtained from a THF solution were of good quality for an X-ray structure determination, which led to the formulation $[CoI_2(\mu\text{-}dppfO_2)]_n$, **3**. The Cp ring is lost and the oxidised dppf coordinates through the oxygen atom, in a bridging manner, joining tetrahedral Co(II) units and giving rise to a polymeric chain (see Scheme 2).

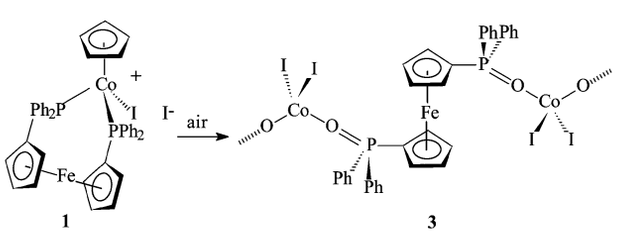

1 **3**

Scheme 2

This result is quite unexpected, since in the similar complexes $[Co(\eta^5\text{-}C_5H_5)(P\text{–}P)I]I$, [P–P = bis(tertiary phosphine)] described in ref. 9 the reaction proceeds in a different way. When solutions of the complexes were exposed to air, the product consisted of the neutral complex $[Co(\eta^5\text{-}C_5H_5)\{(O)P\text{–}P\}I_2]$, with a monodentate (O)P–P ligand bonded to the metal through the phosphorus atom. Some free (O)P–P(O) was also detected.

Although the mechanism of formation of the Co(II) complex **3** from the Co(III) complex **1** is not known, it is certain that the metal complex is required for the oxidation of dppf, since without it, dppf is stable under the same conditions. Although in most known examples the metal keeps its formal oxidation state, it may be thought that upon replacement of P donor ligands by O donor ligands in the coordination sphere of Co(III), the complex is more easily reduced, yielding the Co(II) derivative.

Metal mediated oxidation of phosphines is well known and several mechanisms have been invoked.[10] However, in the reaction described above the ligand dppf itself already contains a metal, and therefore the mechanism of oxidation of dppf could be quite different from that of bis(tertiary phosphines). For instance, $dppfO_2$ can be formed from the electrochemical oxidation of dppf in the presence of solvents with traces of water.[11]

Attempts to obtain compound **3** by the direct reaction of $dppfO_2$ with CoI_2 in CH_2Cl_2 gave instead the monomeric compound $[CoI_2(dppfO_2)]$, **4**, as green crystals, in almost quantitative yield, the ligand $dppfO_2$ being coordinated in a chelating form. The liquid secondary ion mass spectra ($LSIMS^+$) of both compounds **3** and **4** show the base peak at *m*/*z* 772 $[CoI(dppfO_2)]$ (100%). Other fragments, like $[Co(dppfO_2)]$ (*m*/*z* 645) and $dppfO_2$ (*m*/*z* 587), are also found in both complexes. The IR spectra of compounds **3**, and **4**, display strong absorption bands in the region ν 1169–1148 cm^{-1} in Nujol mulls; this is the absorption region for ν(P=O). Uncoordinated $dppfO_2$ displays a strong ν(P=O) absorption at 1168 cm^{-1} in Nujol mull.[3]

Polymeric $[CoI_2(\mu\text{-}dppfO_2)]_n$, **3**, and monomeric $[CoI_2(dppfO_2)]$, **4**, were structurally characterised by single crystal X-ray diffraction studies, as well as the starting material **2**.

Table 1 Selected bond lengths (Å) and angles (°) for complexes **2**, **3**, and **4**

$[CoCp(CO)I_2]$, **2**			
Co–I	2.565(3)	Co–C(1)	1.764(9)
I–Co–I′	94.0(1)	I–Co–C(1)	89.1(2)
		Co–C(1)–O(1)	179.8(9)
$[CoI_2(\mu\text{-}dppfO_2)]_n$, **3**			
Co–I(1)	2.585(3)	Co–O(1)	1.956(9)
Co–I(2)	2.517(3)	Co–O(2)	1.940(8)
P(1)–O(1)	1.497(9)	P(2)–O(2)	1.519(8)
I(1)–Co–I(2)	114.7(12)	O(1)–Co–O(2)	106.9(4)
I(1)–Co–O(1)	107.3(3)	I(1)–Co–O(2)	111.3(3)
I(2)–Co–O(1)	108.7(3)	I(2)–Co–O(2)	107.7(3)
P(1)–O(1)–Co	150.2(6)	P(2)–O(2)–Co	154.5(5)
$[CoI_2(dppfO_2)]$, **4**			
Co–I(1)	2.601(3)	Co–O(1)	1.950(5)
Co–I(2)	2.582(3)	Co–O(2)	1.967(5)
P(1)–O(1)	1.497(5)	P(2)–O(2)	1.504(4)
I(1)–Co–I(2)	117.8(1)	I(1)–Co–O(2)	106.1(1)
I(1)–Co–O(1)	106.3(2)	I(2)–Co–O(1)	109.8(2)
I(2)–Co–O(2)	108.0(1)	O(1)–Co–O(2)	108.4(2)
P(1)–O(1)–Co	167.6(3)	P(2)–O(2)–Co	150.7(3)

Crystallographic studies of $[CoCp(CO)I_2]$, 2, $[CoI_2(\mu\text{-}dppfO_2)]_n$, 3, and $[CoI_2(dppfO_2)]$, 4

The crystal structures of neutral cobalt derivatives of $dppfO_2$, namely, $[CoI_2(\mu\text{-}dppfO_2)]_n\cdot 0.5THF$, **3**·0.5THF, and $[CoI_2(dppfO_2)]\cdot CH_2Cl_2$, **4**·$CH_2Cl_2$, and of the starting material $[CoCp(CO)I_2]$, **2**, were determined by X-ray diffraction. Selected bond distances and angles in the cobalt coordination sphere are given in Table 1 for complexes **2**, **3**, and **4**, respectively.

The crystal structure of **3** is formed by one-dimensional chains of CoI_2O_2 distorted tetrahedral units, covalently linked by $dppfO_2$ bridges and THF solvate molecules. The asymmetric unit consists of one $[CoI_2(dppfO_2)]$ moiety and one independent THF solvent molecule with the occupation factor set to 0.50, which was assigned in order to give reasonable temperature factors for the atoms. Fig. 1 presents the overall geometry of one 1-D polymeric chain with the labelling scheme adopted.

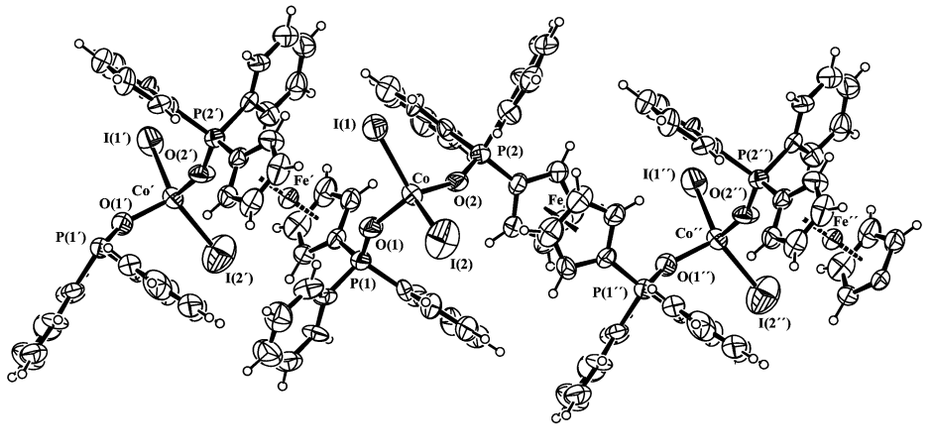

Fig. 1 An ORTEP view of the one-dimensional chain of $[CoI_2(\mu\text{-}dppfO_2)]_n$, **3**, showing its overall geometry and the labelling scheme adopted (40% thermal ellipsoids; ′ denotes the symmetry operation: $x, -y + 0.5, z + 0.5$).

$\{CoI_2O_2\}$ tetrahedral units are connected by $dppfO_2$ bridges, with P–O distances of 1.497(9) and 1.519(8) Å, and Co–O–P angles of 150.2(6) and 154.5(5)°, respectively. The chain has a crystallographically imposed centrosymmetric structure.

The crystal structure of complex **4** consists of discrete $[CoI_2(dppfO_2)]$ complex units and CH_2Cl_2 solvent molecules. The molecular structure of this binuclear complex, including the labelling scheme adopted, is shown in Fig. 2. As found for

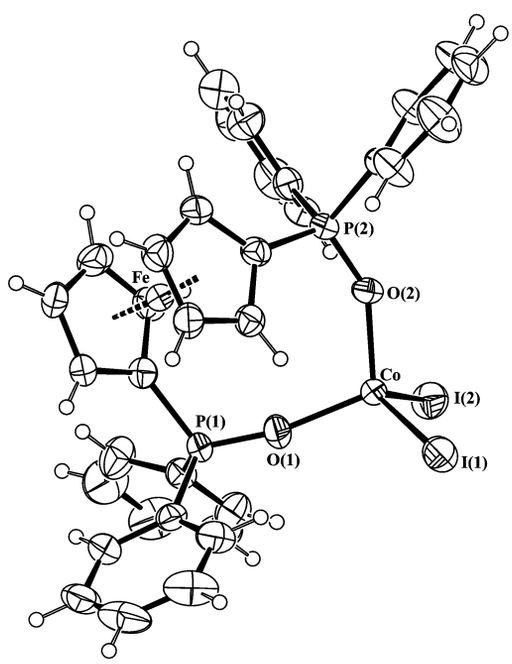

Fig. 2 An ORTEP view of the molecular structure of $[CoI_2(dppfO_2)]$, **4**, with labelling scheme adopted (40% thermal ellipsoids).

complex **3**, two oxygen atoms from a $dppfO_2$ ligand and two iodine atoms define a distorted tetrahedral arrangement around the cobalt centre. However, in the latter complex, the $dppfO_2$ acts as a chelating ligand, adopting a *cis*-configuration. In **3** $dppfO_2$ coordinates in a bridging mode with a *trans*-configuration. Furthermore, the chelating behaviour of $dppfO_2$ results in an almost eclipsed arrangement for the $FeCp_2$ unit, with an α torsion angle between the centroids of two Cp rings and the carbon atoms bound to the phosphorus of 73.2°. Another related complex with a comparable distorted tetrahedral geometric arrangement is $[PdCl_2(dppfO_2)]$,[12] which has an α torsion angle of 79.3° and Pd–O distances of 1.968 and 1.974 Å, respectively. In complex **3**, on the other hand, the $FeCp_2$ units display an almost staggered conformation with a torsion angle of 178.4°. The angles subtended at the cobalt centre(s) and the distances have comparable values in **3** and **4**.

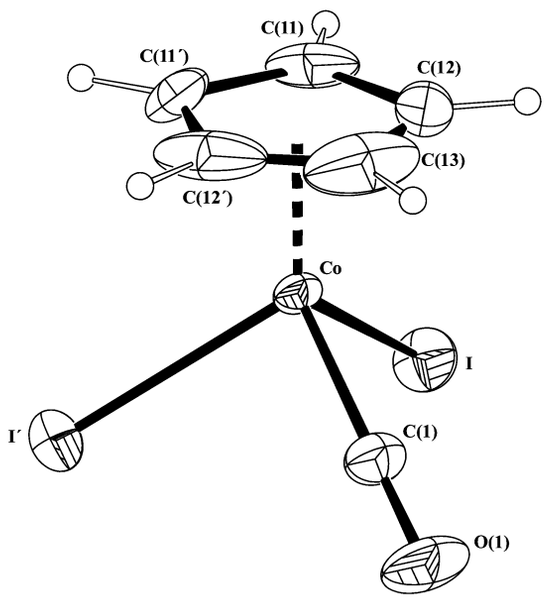

Fig. 3 An ORTEP view of the molecular structure of $[CoCp(CO)I_2]$, **2**, with labelling scheme adopted (40% thermal ellipsoids; ′ denotes the symmetry operation: $x, -y + 0.5, z$).

Fig. 3 depicts the molecular structure of the starting material $[CoCp(CO)I_2]$, **2**, showing the cobalt centre bound to the η^5-Cp ring, one carbonyl and two iodine atoms, in a pseudo tetrahedral coordination environment. The molecule contains a crystallographic symmetry plane running through the carbonyl ligand and the cobalt(II) centre leading to equal Co–I distances of 2.565(3) Å, which are similar to those found for complex **3**.

Magnetic properties of $[CoI_2(\mu\text{-}dppfO_2)]_n$, 3, and $[CoI_2(dppfO_2)]$, 4

In the case of the polymeric $[CoI_2(\mu\text{-}dppfO_2)]_n$ and monomeric $[CoI_2(dppfO_2)]$ compounds, the magnetic susceptibility, χ, temperature dependence and the magnetisation field dependence at low temperatures were studied. The temperature dependence of the χT product is shown in Fig. 4, for polycrystalline samples with an applied field of 5 T and both compounds present a similar χT temperature dependence. The obtained effective magnetic moments, 4.50 and 4.53 μ_B for $[CoI_2(dppfO_2)]$ and $[CoI_2(\mu\text{-}dppfO_2)]_n$, respectively, are in good agreement with the values reported for tetrahedral high spin compounds.[13] The paramagnetic susceptibility deviates considerably from a simple Curie behaviour, $\chi = C/T$, as can be observed in Fig. 4 through the presence of a maximum in χT at *ca.* 30 K *and* a minimum at *ca.* 120 K.

Table 2 Summary of the results from the fits for $[CoI_2(dppfO_2)]$, **4**, $[CoI_2(\mu\text{-}dppfO_2)]_n$, **3**, $[CoCl_2(PPh_3)_2]$, and $[CoBr_2(PPh_3)_2]$ using eqns. (1)–(3)

Compound	ϕ/°	g_z	$g_\perp$	Dk^{-1}/K	TIP/emu mol^{-1}	θ/K
$[CoI_2(dppfO_2)]$, **4**	43.5	2.25	2.24	−13.0	4.97×10^{-4}	
$[\{CoI_2(\mu\text{-}dppfO_2\}_n]$, **3**	38.4	2.26	2.27	−14.0	4.69×10^{-4}	
$[CoCl_2(PPh_3)_2]$		2.21	2.20	−17.9	5.36×10^{-4}	−2.02
$[CoBr_2(PPh_3)_2]$		2.32	2.20	−24.1	6.10×10^{-4}	−1.86

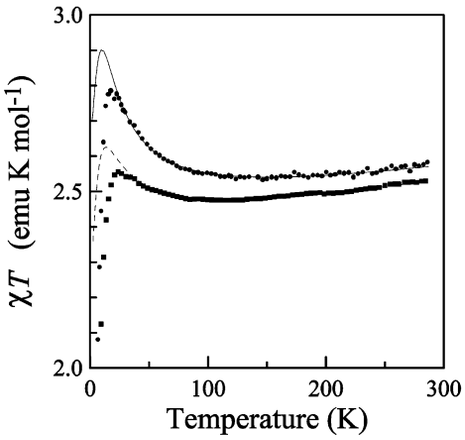

Fig. 4 χT temperature dependence of $[CoI_2(\mu\text{-}dppfO_2)]_n$, **3**, (●) and $[CoI_2(dppfO_2)]$, **4**, (■). Fits to the experimental results are represented by the solid and dashed lines, for **3** and **4**, respectively (see text).

The non-Curie behaviour is consistent with the existence of a strong paramagnetic anisotropy due to zero field splittings (ZFS), which are common on Co^{II} $S = 3/2$ tetrahedral compounds,[14] together with orientation effects due to the strong external applied magnetic field, and with a temperature independent paramagnetic (TIP) contribution. At high temperatures ($120 < T < 300$ K), the behaviour of χT is dominated by the TIP contribution. The increase of χT, below 120 K, is attributed to a partial alignment of the crystals with the applied field that originates a dominance of the parallel susceptibility in relation to the perpendicular component, which for the $^4A_2$, $S = 3/2$, electronic state are given by ref. 14:

$$\chi_{\parallel} = \frac{Ng_z^2\mu_B^2}{4KT}\left(\frac{1+9\exp(-2x/T)}{1+\exp(-2x/T)}\right) \quad (1)$$

$$\chi_{\perp} = \frac{Ng_\perp^2\mu_B^2}{kT}\left(\frac{1}{1+\exp(-2x/T)} + \frac{3T\tanh(x/T)}{4x}\right) \quad (2)$$

where N is Avogadro's number, μ_B is the Bohr magneton, k is the Boltzmann constant, g_z and $g_\perp$ are the parallel and perpendicular components of the g factor, $x = D/k$ and D is the ZFS parameter. At lower temperatures ($T < 30$ K), the fast decrease in χT is attributed to the non-linear field dependence of the magnetization for large values of H/T. This is consistent with the position of the maximum, which was observed to shift to lower temperatures with smaller applied fields. At 1.7 K, the magnetization nearly saturates for $H \geq 2$ T, at $M_S \approx 3N\mu_B$.

The solid and dashed lines in Fig. 4 represent the fits for compounds **3** and **4**, respectively, taking into account the orientation effect on the susceptibility, through eqns. (1) and (2), plus a TIP contribution:

$$\chi = \cos^2(\varphi)\chi_{\parallel} + \sin^2(\varphi)\chi_{\perp} + \text{TIP} \quad (3)$$

the obtained parameters are shown in Table 2 and compared with the ones from single crystal measurements obtained with other Co^{II} $S = 3/2$ tetrahedral compounds, such as $[Co(PPh_3)_2Cl_2]$ and $[Co(PPh_3)_2Br_2]$,[15] where negative zero field splitting was also observed.[16] In the case of these last compounds the existence of antiferromagnetic interactions were considered since they show AFM ordering at low temperatures,[16] while in the case of $[CoI_2(dppfO_2)]_n$ and $[CoI_2(dppfO_2)]$, the low temperature magnetic field dependence, closely following the Brillouin function calculated values, indicates that the magnetic interactions can be neglected.

Electrochemical studies

Fig. 5 shows the rather complex redox pattern exhibited in cyclic voltammetry by the Co(III) derivative $[Co(\eta^5\text{-}C_5H_5)(dppf\text{-}P,P')]I$, **1**, in dichloromethane solution.

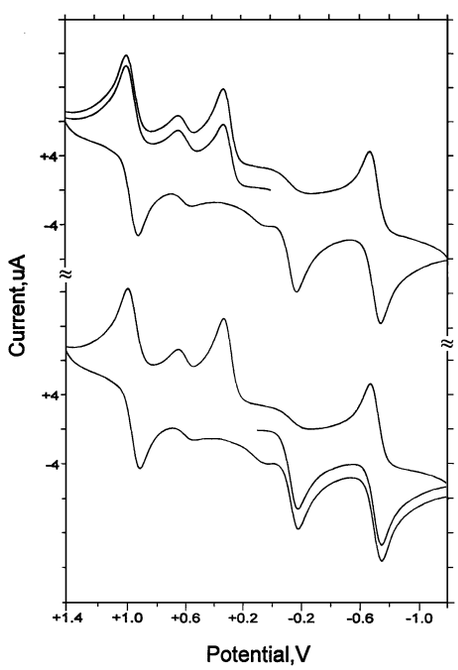

Fig. 5 Cyclic voltammetric responses recorded, under opposite scan directions, at a platinum electrode on a CH_2Cl_2 solution containing $[Co(\eta^5\text{-}C_5H_5)(dppf\text{-}P,P')]I$ (1.2×10^{-3} mol dm^{-3}) and $[NBu_4][PF_6]$ (0.2 mol dm^{-3}). Scan rate 0.2 V s^{-1}.

As seen, the overall redox profile is independent from the scan direction. In this light, let us first discuss the anodic path. The two processes occurring in the range from 0 to 0.7 V are typical of free iodide ions[17] and are hence assigned to the oxidation of the iodide counteranion. The further reversible oxidation at about 1 V is conceivably due to the oxidation of dppf ligand. As a matter of fact, analysis[18] of such response with scan rate varying from 0.02 to 0.5 V s^{-1}, shows that the current ratio i_{pc}/i_{pa} is constantly equal to 1, the current function $i_{pa}v^{-1/2}$ remains substantially constant, the peak-to-peak separation increases from 65 to 72 mV. It is useful to note that under the same experimental conditions the (first) oxidation of free dppf occurs at +0.57 V. In this connection, anodic shifts of about 0.4 V have been also observed for the Co(III)-dppf complexes $[Co(acac)_2(dppf)]^+$[19] and $[Co(NO)_2(dppf)]^+$,[20] which point

Table 3 Formal electrode potentials (in V, *vs.* SCE) for the redox changes exhibited by the present cobalt–dppf and cobalt–dppfO_2 complexes in dichloromethane solution

Species	Oxidation processes					Reduction processes	
	$E^{o\prime\,a}$	$E^{o\prime\,a}$	$E^{o\prime\,b}$	$E^{o\prime\,c}$	$E^{o\prime\,d}$	$E^{o\prime\,e}$	$E^{o\prime\,f}$
[CpCoI(dppf)]I	+0.30[g]	+0.57	—	+0.94	—	−0.20[g]	−0.72
[CpCoI_2(CO)]	—	—	—	—	+1.25[g]	−0.06	−0.85[g]
[CoI_2(dppfO_2)]	—		—	+0.44[g]	+1.08	—	—
dppf	—	—	—	+0.57	—	—	—
dppfO_2	—	—	—	+0.82[h]	—	—	—
[NBu_4]I	+0.18	+0.57	—	—	—	—	—

[a] Oxidation of free I^- ions. [b] Co(II)/Co(III) oxidation. [c] Oxidation of the ferrocene-based ligand. [d] Oxidation of coordinated halogen. [e] Co(III)/Co(II) reduction. [f] Co(II)/Co(I) reduction. [g] Peak potential values for processes coupled to fast chemical complications; measured at 0.2 V s^{-1}. [h] From ref. 11.

out the high affinity of cobalt fragments towards the dppf ligand.

Less straightforward appears the attribution of the cathodic path. From a qualitative viewpoint the two consecutive reduction processes are preliminarily assigned to the sequence Co(III)/Co(II)/Co(I), also in view of the behaviour exhibited by the parent Co(III) derivative [Co(η^5-C_5H_5)(CO)I_2], which displays a first, partially reversible reduction at about −0.1 V and a further irreversible reduction at about −0.8 V. As the actual first reduction step does not display any associated reoxidation peak even at 20 V s^{-1}, it must be taken into account that the corresponding exhaustive reduction of the original red solution of [Co(η^5-C_5H_5)(dppf-*P*,*P*′)I]I (E_w = −0.4 V) consumes one-electron/molecule, and the resulting yellow–orange solution exhibits in cyclic voltammetry a redox profile substantially similar to that illustrated in Fig. 5, but for the disappearance of the first irreversible reduction and the increase of free iodide oxidation. A possible mechanism for the reduction sequence could therefore be formulated as:

$$[Co^{III}(C_5H_5)(dppf)I]^+ \xrightarrow{+e^-} [Co^{II}(C_5H_5)(dppf)I] \xrightarrow[-I^-]{\text{fast}} [Co^{II}(C_5H_5)(dppf)]^+$$

$$[Co^{II}(C_5H_5)(dppf)]^+ \overset{-e^- \uparrow\downarrow +e^-}{\rightleftharpoons} [Co^{I}(C_5H_5)(dppf)]$$

The formal electrode potentials of the above discussed redox changes are compiled in Table 3.

Let us now pass to the dppfO_2–Co(II) derivative [CoI_2(dppfO_2)], **4**. As illustrated in Fig. 6, it exhibits a rather complex voltammetric pattern.

A first oxidation at about +0.4 V, which is accompanied by almost overlapping minor processes, precedes a further better defined anodic process at about + 1 V, which possesses features of chemical reversibility. The picture is best defined by the Osteryoung Square Wave Voltammogram (OSWV). Since controlled potential coulometry in correspondence to the first anodic step indicated the consumption of about 1.2 electrons per molecule, we assume that [CoI_2(dppfO_2)] undergoes at first the Co^{II}/Co^{III} oxidation followed in turn by the dppfO_2–Fe^{II}/Fe^{III} oxidation. The minor complications accompanying the Co^{II}/Co^{III} step are likely due to free iodide ions, which can be present in traces as complications either preceding (slight dissociation of the original complex) or following the electron transfer. From a speculative viewpoint, we point out that the shift induced in the oxidation potential of the dppfO_2 ligand with respect to free dppfO_2 is significantly smaller than that observed for dppf in $[Co^{III}(C_5H_5)(dppf)I]^+$ (0.26 *vs.* 0.37 V), likely precluding a slightly lower affinity of dppfO_2 with respect to dppf towards cobalt coordination.

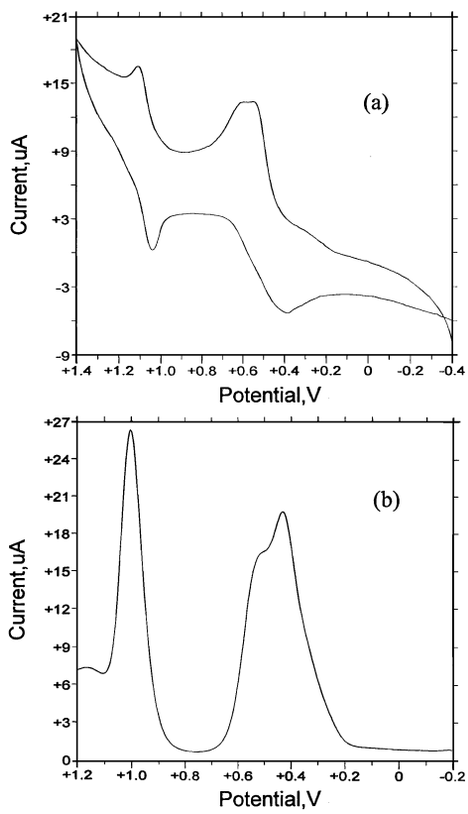

Fig. 6 Cyclic (a) and OSWV (b) voltammograms recorded at a platinum electrode on a CH_2Cl_2 solution containing [Co(dppfO_2)I_2] (1.1×10^{-3} mol dm^{-3}) and [NBu_4][PF_6] (0.2 mol dm^{-3}). Scan rates (a) 0.02 V s^{-1}; (b) 0.1 V s^{-1}.

Molecular orbital study of [Co(η^5-C_5H_5)(dppf-*P*,*P*′)I]I, 1, the polymeric chain [CoI_2(μ-dppfO_2)]$_n$, 3, [CoI_2(dppfO_2)], 4, and some related complexes

DFT calculations[4] (ADF program)[5] were performed on some of the complexes studied. The simplest is the diamagnetic Co(III) cationic complex, [Co(η^5-C_5H_5)(dppf-*P*,*P*′)I]$^+$, **1**, for which a full geometry optimization was carried out, using a model based on the structures of the other complexes described above. The optimized structure is shown in Fig. 7. The distances and angles are similar to those found in this type of complex. The P–Co–P and P–Co–I angles are very close to 90°, showing how this part of the molecule approaches a half octahedron. The Co ··· Fe distance is 4.159 Å, the only communication between metals being through the bridging ligands.

The HOMO and the HOMO − 1 of this complex are 82.0 and 78.3% localized on Fe, or 94.8 and 93.2% on the (C_5H_4)Fe fragment, respectively. The LUMO, on the other hand, is concentrated 40.5% on Co, 24.6% on I, and 5.5% on the two P atoms, the LUMO + 1 being comparable. These compositions

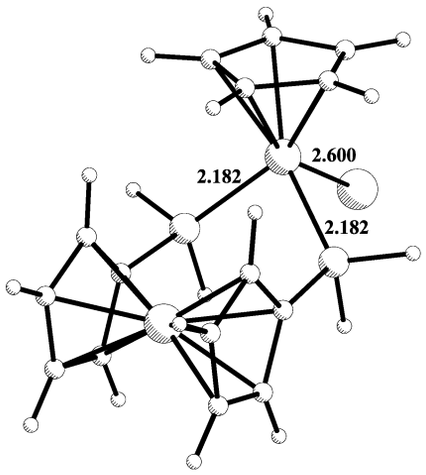

Fig. 7 The fully optimized geometry of $[Co(\eta^5\text{-}C_5H_5)(dppf\text{-}P,P')I]^+$, **1**, with some relevant distances (Å).

agree extremely well with the proposed redox processes for oxidation and reduction (see above).

The other complex studied by cyclic voltammetry was the paramagnetic Co(II) derivative $[CoI_2(dppfO_2)]$ and spin unrestricted DFT calculations were performed. The optimized structure can be compared with the experimental crystal structure so that the reliability of the calculational method can be evaluated, as seen in Fig. 8.

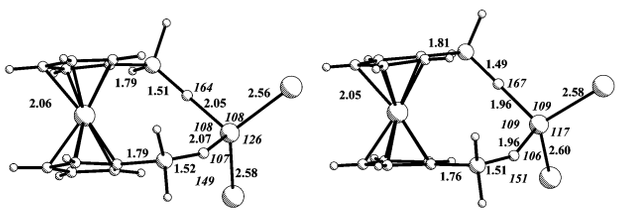

Fig. 8 The fully optimized geometry of $[CoI_2(dppfO_2)]$, **4**, DFT (left) and the X-ray structure (right), with some relevant distances (Å) and angles (°, italics).

The agreement between the calculated and the experimental structures is very good, both for distances and angles. The only parameter which deviates significantly is the I–Co–I angle (126° calc.; 117° exp.). The calculated spin density for this complex resides mostly on the Co atom (2.527), the second largest contributions being those of the two iodines (0.207, 0.192). All the other atoms contribute almost nothing to the spin density. This indicates that the three highest singly occupied molecular orbitals (SOMOs) have a strong contribution from cobalt, which behaves as a typical tetrahedral Co(II) centre. In order to get a simpler picture of the molecular orbitals, a single point restricted calculation was also performed. The five highest occupied molecular orbitals are essentially Co d orbitals (71.4 to 84.7%). The contribution of Fe to these orbitals goes up to 1.4, 2.1, and 2.8% in the SOMOs of this iodine derivative. The contribution of iodine to the mainly Co d orbitals is relatively large (11.3, 26.8, 24.2, 18.4, 21.7%). It is difficult to predict exactly, from these results, what happens during the oxidation processes, though in principle Fe should not be involved. On the other hand, the LUMOs are strongly localized on Fe and reduction should involve the ferrocenyl moiety. Also, the characterization of the magnetic properties of the iodine complexes as being identical to those of tetrahedral d^7 Co complexes is consistent with the previous description of the molecular levels.

The polymeric chain $[CoI_2(\mu\text{-}dppfO_2)]_n$, **3**, was initially studied as a one-dimensional polymer, using the extended Hückel method[6] with the tight-binding approach.[7] It was found that the bands were extremely flat, so that the unit cell of the polymer, when conveniently ended, provides a good molecular model that can be used to study accurately the electronic structure of this compound. DFT calculations were thus performed for a model $[CoI_2(\mu\text{-}dppfO_2)_2]$, extracted from the chain and with the phenyl groups replaced by hydrogen atoms. This new species resembles $[CoI_2(dppfO_2)]$ in that Co(II) has the same coordination environment, but differs because $dppfO_2$ binds as a monodentate rather than a chelate ligand. The energy levels are shifted to lower energies compared to those of $[CoI_2(dppfO_2)]$, but the spin density is strongly localized in Co (2.507), with a strong contribution of iodine (0.208, 0.191). Iron, as low spin d^6 Fe(II), contributes significantly to the LUMO, the t_{2g} type orbitals being stabilized relative to the Co d levels. This qualitative bonding model agrees with the experimental findings concerning the magnetic behaviour of the polymeric chain, which assigns the magnetic properties to a cobalt(II) centre.

Conclusions

A new Co(III) complex, $[Co(\eta^5\text{-}C_5H_5)(dppf\text{-}P,P')I]$, **1**, was prepared and characterised by multinuclear NMR spectroscopy. Upon exposure to air of solutions of compound **1**, a polymeric chain containing bridging $dppfO_2$ units joining tetrahedral Co(II) centres, $[CoI_2(\mu\text{-}dppfO_2)]_n$, **3**, was formed. In an attempt to obtain **3** *via* a different route, direct reaction of $dppfO_2$ with CoI_2, was checked and found instead to lead to the monomeric $[CoI_2(dppfO_2)]$, **4**, with $dppfO_2$ as a chelate. The structures of these Co(II) derivatives were confirmed by single crystal X-ray diffraction. The electrochemical study showed that the Co(III) species was reduced to Co(II), followed by loss of iodine and further reduction to Co(I). DFT calculations led to a calculated structure and an electronic structure which was consistent with the electrochemical data. The derivatives **3** and **4** behaved as tetrahedral $S = 3/2$ Co^{II}, possessing a $^4A_2$ ground state, and $S = 0$ Fe^{II} complexes with three unpaired electrons, when their magnetic behaviour was investigated and temperature dependence of the magnetic susceptibility analysed $\{D/k = -13$ and -14 K for $[CoI_2(dppfO_2)]$ and $[CoI_2(\mu\text{-}dppfO_2)]_n$, respectively$\}$.

Comparison of the electrochemical behaviour of $[Co^{III}(\eta^5\text{-}C_5H_5)(dppf)I]^+$ and $[Co^{II}I_2(dppfO_2)]$ with that of the respective free diphenylphosphinoferrocene ligands (namely, dppf and $dppfO_2$) suggests that the oxygenated diphosphine has a lower affinity towards cobalt coordination.

Experimental

General procedures and materials

All reactions and manipulations of solutions, except for the exposure to air experiments, were performed under an argon atmosphere using Shlenck techniques. Solvents were of reagent grade and were dried according to literature methods. CoI_2 was purchased from Aldrich and $Co_2(CO)_8$ was purchased from Fluka and were used as supplied.

Physical methods

Infrared spectra were recorded as mulls on NaCl plates using an ATI Mattson Genesis FTIR spectrometer. Elemental analyses were performed at the microanalytical laboratory of the Universidade Técnica de Lisboa, Portugal. Mass spectra were recorded on a VG Autospec instrument (LSIMS) using 3-nitrobenzylalcohol as matrix and a caesium gun, at the Instituto de Ciencias de Materiales de Aragon, Zaragoza, Spain. NMR samples were recorded on a Bruker ARX 400 using TMS as internal reference. Magnetic susceptibility data of polycrystalline $CoI_2(dppfO_2)$ samples, using a Teflon sample holder, were obtained, in the range 4–300 K, with a longitudinal Faraday system (Oxford Instruments), with a 7 T superconducting magnet, under a magnetic field of 5 T and forward and

reverse gradients fields of 1 T m^{-1}. The force was measured with a microbalance (Sartorius S3D-V). The data were corrected for contributions due to sample holder and core diamagnetism, estimated from tabulated Pascal constants.

Synthesis of complexes

The ligands 1,1′-bis(diphenylphosphino)ferrocene (dppf)[21] and 1,1′-bis(diphenylphosphoranyl)ferrocene ($dppfO_2$)[22] and the complexes $[Co(\eta^5\text{-}C_5H_5)(CO)_2]$[23] and $[Co(\eta^5\text{-}C_5H_5)(CO)I_2]$, **2**,[24] were prepared as previously reported.

$[Co(\eta^5\text{-}C_5H_5)(dppf\text{-}P,P')I]I$, 1. A solution of dppf (0.68 g, 1.2 mmol) in CH_2Cl_2 (25 cm^3) was added to a solution of $[Co(\eta^5\text{-}C_5H_5)(CO)I_2]$, **2**, (0.47 g, 1.2 mmol) in CH_2Cl_2 (50 cm^3), magnetically stirred at room temperature; a colour change was observed from the very dark violet of the initial solution to a red–brown. Gas evolution was immediately observed (presumably CO). The mixture was left stirring for about 30 minutes, the solution was concentrated by removal of the solvent *in vacuo*, petroleum ether (bp 40–60 °C) was added until becoming turbid and the solution was then filtered and left in the refrigerator. After a few days (two or three) brown–reddish crystals formed which were recovered by filtration, washed with petroleum ether (bp 40–60 °C), and dried *in vacuo* to give pure **1**. Yield 0.9 g (80%) (Found: C, 49.97; H, 3.60. Calc. for $C_{39}H_{33}CoFeP_2I_2$: C, 50.23; H, 3.54%). Mass spectrum: *m*/*z* 805 (7%, $M^+ - I$), 678 (100, $M^+ - 2I$), 554 (30, dppf). NMR ($CDCl_3$): ^1H, δ 7.77–7.47 (m, 10H, Ph), 5.3 (s, 2H, C_5H_4), 5.22 (s, 5H, C_5H_5), 4.52 (s, 2H, C_5H_4), 4.48 (s, 2H, C_5H_4), 4.27 (s, 2H, C_5H_4); ^{31}P, δ 47.29 (s).

$[CoI_2(\mu\text{-}dppfO_2)]_n$, 3. Exposure of a CH_2Cl_2 or THF solution of **1** to air resulted in a colour change from red–brown to green in a few days. Green crystal of **3** can be obtained from the green solution; the reaction was repeated several times and although a colour change is always observed it is difficult to obtain crystals and the yields are erratic. A sample obtained when CH_2Cl_2 was used as solvent was used for elemental analyses. (Found: C, 43,26; H, 3.09. Calc. for $C_{35}H_{30}CoFeCl_2P_2O_2I_2$: C, 42.70; H, 3.05%). Mass spectrum: *m*/*z* 772 {100%, $[CoI(dppfO_2)]$}, 645 {45, $[Co(dppfO_2)]$}, 587 (32, $dppfO_2$). IR (Nujol, ν/cm^{-1}): P=O 1169–1148cm^{-1}.

$[CoI_2(dppfO_2)]$, 4. A solution of $dppfO_2$ (0.36 g, 0.6 mmol) in CH_2Cl_2 (15 cm^3) was added to a suspension of CoI_2 (0.19 g, 0.6 mmol) in CH_2Cl_2 (30 cm^3), magnetically stirred at room temperature, a bright green solution formed which was left stirring for 1 hour, at which point the solution was filtered and concentrated by vacuum removal of the solvent until becoming turbid. The solution was then filtered and left in the refrigerator whereupon green crystals formed; they were separated by filtration and recrystallized from CH_2Cl_2–petroleum ether (bp 40–60 °C) to give well formed crystals of **4**. The yield was essentially quantitative (Found: C, 43.15; H, 2.90. Calc. for $C_{35}H_{30}CoFeCl_2P_2O_2I_2$: C, 42.70; H, 3.05%). Mass spectrum: *m*/*z* 772 {100%, $[CoI(dppfO_2)]$}, 645 {32, $[Co(dppfO_2)]$}, 587 (20, $dppfO_2$). IR (Nujol, ν/cm^{-1}): P=O 1169–1148cm^{-1}.

Crystallography

Crystal data together with refinement details for complexes **2**, **3** and **4** are given in Table 4.

The X-ray data were collected on a MAR research plate system using graphite Mo-Kα radiation at Reading University. The crystals were positioned 70 mm from the image plate. 95 frames were taken at 2° intervals using a counting time between 2 and 10 min adequate to the crystal under study. Data analysis was performed with XDS program.[25] Intensities of **2** and **3** were corrected empirically for absorption effects using a version of DIFABS modified for image plate geometry.[26] The structures of complexes **2**, **3**, and **4** were solved by a combination of the direct and difference Fourier syntheses followed by least-squares refinement. After all positions of non-hydrogen atoms of complexes **3** and **4** had been located, it was clear from the Fourier difference maps that the solvent molecules were present in the asymmetric unit of these complexes. Thus, one molecule of THF with an occupancy of 0.50 and one CH_2Cl_2 molecule were found for complexes **3** and **4**, respectively. The occupancy factors of the THF molecule was set to 0.50 in order to give reasonable isotropic thermal parameters and low *R* values. The hydrogen atoms on the carbon atoms were included in calculated positions and given thermal parameters equivalent to 1.2 times those of the atom to which they were attached. All non-hydrogen atoms of the three complexes were refined anisotropically, except the carbon and oxygen atoms of THF molecules, which were refined with individual isotropic temperature factors.

The structures were refined on F^2 until convergence. All calculations required to solve and refine the structures were carried out with SHELXS and SHELXL within the SHELX-97 package.[27] Molecular and crystal packing diagrams were drawn with PLATON.[28]

CCDC reference numbers 164967–164969.

See http://www.rsc.org/suppdata/dt/b2/b205942h/ for crystallographic data in CIF or other electronic format.

Electrochemistry

Materials and apparatus for electrochemistry have been described elsewhere.[29] All the potential values are referred to the Saturated Calomel Electrode (SCE). Under the present experimental conditions the one-electron oxidation of ferrocene occurs at $E^{\circ\prime} = +0.39$ V. *N*,*N*-Dimethyl-1-[1′,2-bis(diphenylphosphino)ferrocenyl]ethylamine was an Aldrich product.

Computational studies

Density functional calculations[4] were carried out with the Amsterdam Density Functional (ADF) program developed by Baerends and co-workers (release 2.3 and ADF-1999).[5] Vosko, Wilk and Nusair's local exchange correlation potential was used,[30] with Becke's nonlocal exchange[31] and Perdew's correlation corrections.[32] The geometry optimization procedure was based on the method developed by Versluis and Ziegler,[33] using the non-local correction terms in the calculation of the gradients, together with non-local exchange and correlation corrections. Unrestricted calculations were performed for paramagnetic species unless otherwise stated. The structures of the complexes described in this work were used to prepare input files for the optimization of the geometry of the model complexes. The model for the chain was obtained by replacing phenyl groups by hydrogen atoms and ending the unit cells with hydrogen atoms. Full optimizations without symmetry constraints were always performed. In all the calculations, a triple-ζ Slater-type orbital (STO) basis set was used for Co and Fe 3s, 3p, 4s, 4p, 3d, as well as for I 5s, 5p; triple-ζ STO augmented with a single-ζ polarization function were used for P 3s and 3p, C, O, 2s and 2p, and H 1s. A frozen core approximation was used to treat the core electrons of C and O (1s), P ([1–2]s, 2p), Co and Fe ([1–2]s, 2p), and I ([1–4]s, [1–4]p, [3,4]d).

Extended Hückel[7] calculations were carried out with modified H_{ij} values,[34] and using the tight-binding approach on polymeric chain **3**.[6] The basis set for the metal atoms consisted of *n*s, *n*p and (n − 1)d orbitals. The s and p orbitals were described by single Slater-type wave functions, and the d-orbitals were taken as contracted linear combinations of two Slater-type wave functions. The parameters used were [H_{ii} (eV), ζ]: Co 4s −9.21, 2.000; 4p −5.29, 2.000; 3d −13.18, 5.55, 2.100 (ζ_2), 0.5679 (C_1), 0.6059 (C_2); Fe 4s −9.100, 1.900; 4p −5.32, 1.900; 3d −12.60, 5.35, 2.000 (ζ_2), 0.5505 (C_1), 0.6260 (C_2); I 5s −18.00, 2.679; 5p −12.700, 2.322. Standard parameters were used for other atoms. The program YAeHMOP was used in calculations.[35]

Table 4 X-Ray room temperature data and structure refinement details for complexes $[CoCp(CO)I_2]$, **2**, $[CoI_2(\mu\text{-dppfO}_2)]_n$, **3**, and $[CoI_2(dppfO_2)]$, **4**

Compound	**2**	**3**·0.5THF	**4**·CH_2Cl_2
Empirical formula	$C_6H_5CoI_2O$	$C_{36}H_{32}CoFeI_2O_{2.5}P_2$	$C_{34}H_{28}CoFeI_2O_2P_2\cdot CH_2Cl_2$
M	405.83	935.14	984.01
Crystal system	Monoclinic	Monoclinic	Monoclinic
Space group	$P2_1/m$	$P2_1/c$	$P2_1/n$
a/Å	6.730(12)	12.922(17)	11.371(15)
b/Å	11.167(17)	20.001(29)	17.971(25)
c/Å	7.033(12)	17.820(25)	18.211(25)
β/°	117.49(1)	110.66(1)	91.04(1)
V/Å^3	468.9	4309.4	3720.8
Z	2	4	4
D_c/g cm^{-3}	2.875	1.441	1.757
μ/mm^{-1}	8.350	2.255	2.755
Reflections collected	1358	12554	10861
Independent reflections	832	7540	6211
R_{int}	0.0323	0.0615	0.0256
Final R indices			
R_1, wR_2 [$I > 2\sigma(I)$]	0.0378, 0.1050	0.0974, 0.2782	0.0454, 0.1066
R_1, wR_2 (all data)	0.0389, 0.1063	0.1904, 0.3254	0.0804, 0.1212

Acknowledgements

This work was partially supported by PRAXIS XXI (2/2.1/QUI/419/94 and PRAXIS/PCNA/C/QUI/103/96). P. Zanello gratefully acknowledges the financial support from the University of Siena (PAR 2001). T. A., M. J. C. and P. Z. thank the bilateral program CNR/ICCTI for funding. Thanks are given to Prof. Mariano Laguna from the Instituto de Ciencias de Materiales de Aragon for the mass spectra. We thank the EPSRC and the University of Reading for funds for the Image Plate system.

References

1 (*a*) A. Togni and T. Hayashi, *Ferrocenes*, VCH, Weinheim, 1995; (*b*) F. H. Allen and O. Kennard, *Chem. Des. Autom. News*, 1993, **8**, 31.
2 M. Adachi, M. Kita, K. Kashiwabara, J. Fujita, N. Iitaka, S. Kurachi, S. Ohba and D.-M. Jin, *Bull. Chem. Soc. Jpn.*, 1992, **65**, 2037.
3 (*a*) G. Pilloni, G. Valle, C. Corvaja, B. Longato and B. Corain, *Inorg. Chem.*, 1995, **34**, 5910; (*b*) P. Pinto, M. J. Calhorda, V. Felix, T. Avilés and M. G. B. Drew, *Monatsh. Chem.*, 2000, **131**, 1253.
4 R. G. Parr and W. Yang, *Density Functional Theory of Atoms and Molecules*, Oxford University Press, New York, 1989.
5 (*a*) ADF(1999), E. J. Baerends, A. Bérces, C. Bo, P. M. Boerrigter, L. Cavallo, L. Deng, R. M. Dickson, D. E. Ellis, L. Fan, T. H. Fischer, C. Fonseca Guerra, S. J. A. van Gisbergen, J. A. Groeneveld, O. V. Gritsenko, F. E. Harris, P. van den Hoek, H. Jacobsen, G. van Kessel, F. Kootstra, E. van Lenthe, V. P. Osinga, P. H. T. Philipsen, D. Post, C. C. Pye, W. Ravenek, P. Ros, P. R. T. Schipper, G. Schreckenbach, J. G. Snijders, M. Sola, D. Swerhone, G. te Velde, P. Vernooijs, L. Versluis, O. Visser, E. van Wezenbeek, G. Wiesenekker, S. K. Wolff, T. K. Woo and T. Ziegler, Vrije Universiteit, Amsterdam, The Netherlands, 1999; (*b*) C. Fonseca Guerra, O. Visser, J. G. Snijders, G. te Velde and E. J. Baerends, *Parallelisation of the Amsterdam Density Functional Programme* in *Methods and Techniques for Computational Chemistry*, E. Clementi and C. Corongiu, eds., STEF, Cagliari, 1995, pp. 303–395; (*c*) C. Fonseca Guerra, J. G. Snijders, G. te Velde and E. J. Baerends, *Theor. Chem. Acc.*, 1998, **99**, 391; (*d*) E. J. Baerends, D. Ellis and P. Ros, *Chem. Phys.*, 1973, **2**, 41; (*e*) E. J. Baerends and P. Ros, *Int. J.Quantum Chem.*, 1978, **S12**, 169; (*f*) P. M. Boerrigter, G. te Velde and E. J. Baerends, *Int. J. Quantum Chem.*, 1988, **33**, 87; (*g*) G. te Velde and E. J. Baerends, *J. Comp. Phys.*, 1992, **99**, 84.
6 (*a*) M. H. Whangbo and R. Hoffmann, *J. Am. Chem. Soc.*, 1978, **100**, 6093; (*b*) M. H. Whangbo, W. M. Walsh, jun., R. C. Haddon and E. Wudl, *Solid State Commun.*, 1982, **43**, 637; (*c*) M. H. Whangbo, J. M. Williams, M. A. Beno and J. R. Dorfman, *J. Am. Chem. Soc.*, 1983, **105**, 645.
7 (*a*) R. Hoffmann, *Chem. Phys.*, 1963, **39**, 1397; (*b*) R. Hoffmann and W. N. Lipscomb, *J. Chem. Phys.*, 1962, **36**, 2179.
8 J.-F. Ma and Y. Yamamoto, *J. Organomet. Chem.*, 1999, **574**, 148.
9 Q.-B. Bao, S. J. Landon, A. L. Rheingold, T. M. Haller and T. B. Brill, *Inorg. Chem.*, 1985, **24**, 900.
10 (*a*) A. Sen and J. Halpern, *J. Am. Chem. Soc.*, 1977, **99**, 8337; (*b*) V. M. Miskowski, J. L. Robbins, G. S. Hammond and H. B. Gray, *J. Am. Chem. Soc.*, 1976, **98**, 2477; (*c*) J. B. Birk, J. Halpern and A. L. Pickard, *J. Am. Chem. Soc.*, 1968, **90**, 4491; (*d*) D. D. Schmidt and J. T. Yoke, *J. Am. Chem. Soc*, 1971, **93**, 637.
11 G. Pilloni, B. Longato and B. Corain, *J. Organomet. Chem*, 1991, **420**, 57.
12 J. S. L. Yeo, J. J. Vittal and T. S. A. Hor, *Chem. Commun.*, 1999, 1477.
13 R. L. Carlin, *Magnetochemistry*, Springer-Verlag, Berlin, 1986.
14 R. L. Carlin, *Science*, 1985, **227**, 4692.
15 J. E. Davies, M. Gerloch and D. J. Phillips, *J. Chem. Soc., Dalton Trans.*, 1979, 1836.
16 R. L. Carlin, R. D. Chirico, E. Sinn, G. Mennenga and L. J. de Jongh, *Inorg. Chem.*, 1982, **21**, 2218.
17 G. Dryhurst and P. J. Elving, *Anal. Chem.*, 1967, **39**, 606–615 and references therein.
18 E. R. Brown and J. R. Sandifer, in *Physical Methods of Chemistry, Electrochemical Methods*, B. W. Rossiter and J. F. Hamilton, eds., Wiley, New York, 1986, vol. 2, ch. 4.
19 M. Adachi, M. Kita, K. Kashiwabara, J. Fujita, N. Iitaka, S. Kurachi, S. Ohba and D. Jin, *Bull. Chem. Soc. Jpn.*, 1992, **65**, 2037–2044.
20 A. E. Gerbase, E. J. S. Vichi, E. Stein, L. Amaral, A. Vasquez, M. Horner and C. Maichle-Mössmer, *Inorg. Chim. Acta*, 1997, **266**, 19–27.
21 J. J. Bishop, A. Davison, M. L. Katcher, D. W. Lichtenberg, R. E. Merrill and J. C. Smart, *J. Organomet. Chem.*, 1971, **27**, 241.
22 W. E. Slinkard and D. W. Meek, *J. Chem. Soc., Dalton Trans.*, 1973, 1024.
23 M. D. Rausch and R. A. Genetti, *J. Org. Chem.*, 1970, **35**, 3888.
24 R. B. King, *Inorg. Chem.*, 1966, **5**, 82.
25 W. Kabsch, *J. Appl. Crystallogr.*, 1988, **21**, 916.
26 DIFABS, N. Walker and D. Stuart, *Acta Crystallogr., Sect. A*, 1983, **39**, 158.
27 G. M. Sheldrick, SHELX-97, University of Göttingen, Germany, 1997.
28 A. L. Spek, PLATON, A Multipurpose Crystallographic tool, Utrecht University, Utrecht, The Netherlands, 1999.
29 P. Zanello, F. Laschi, M. Fontani, C. Mealli, A. Ienco K. Tang, X. Jin and L. Li, *J. Chem. Soc., Dalton Trans.*, 1999, 965.
30 S. H. Vosko, L. Wilk and M. Nusair, *Can. J. Phys.*, 1980, **58**, 1200.
31 A. D. Becke, *J. Chem. Phys.*, 1987, **88**, 1053.
32 (*a*) J. P. Perdew, *Phys. Rev.*, 1986, **B33**, 8822; (*b*) J. P. Perdew, *Phys. Rev.*, 1986, **B34**, 7406.
33 (*a*) L. Versluis and T. Ziegler, *J. Chem. Phys.*, 1988, **88**, 322; (*b*) L. Fan and T. Ziegler, *J. Chem. Phys.*, 1991, **95**, 7401.
34 J. H. Ammeter, H.-J. Bürgi, J. C. Thibeault and R. Hoffmann, *J. Am. Chem. Soc.*, 1978, **100**, 3686.
35 G. A. Landrum, YAeHMOP: Yet Another extended Hückel Molecular Orbital Package, YAeHMOP is available on the WWW at: http://yaehmop.sourceforge.net.